Interpretation of relativistic $(e,2e)$ experiments in coplanar asymmetric geometry: Atomic-number-dependent effects

S. Keller,[1,*] R. M. Dreizler,[1] L. U. Ancarani,[2] H. Ast,[1] H. R. J. Walters,[3] and C. T. Whelan[4]
[1]*Institut für Theoretische Physik, Universität Frankfurt, Robert Mayer-Straße 8-10, D-60054 Frankfurt, Germany*
[2]*Laboratoire de Physique Moléculaire et des Collisions, Institute de Physique, Technopôle 2000, 57078 Metz, France*
[3]*Department of Applied Mathematics and Theoretical Physics, The Queen's University of Belfast, Belfast BT7 1NN, United Kingdom*
[4]*Department of Applied Mathematics and Theoretical Physics, University of Cambridge, Cambridge CB3 9EW, United Kingdom*
(Received 25 August 1998)

Triply differential cross sections and spin asymmetries for $(e,2e)$ reactions of the $1s_{1/2}$ state of intermediate- and high-Z atoms in coplanar asymmetric geometry are analyzed within the framework of the relativistic distorted wave Born approximation. Specific signatures of the relativistic nature of the electron-electron interaction, and of the atomic-number-dependent electron-residual ion interaction, are identified. [S1050-2947(99)05902-8]

PACS number(s): 34.80.Dp

I. INTRODUCTION

Total or low-order differential cross sections for inner shell ionization of atoms with high atomic number Z by relativistic electrons have been the subject of theoretical investigations since the early days of quantum mechanics. Already the first studies [1,2] suggest that this process can be treated in perturbation theory, but that it is mandatory to take into account the relativistic nature of the interaction between the incident and the initially bound electron. Indeed, the perturbative approach yields qualitative and in many cases quantitative agreement between calculated and measured inner shell total and singly differential cross sections for a wide range of impact energies and target species [3]. The situation changed when triply differential cross sections (TDCS), obtained by coincident energy and angle resolved detection of the two active electrons, became available [4]. Theoretical attempts (reviewed, e.g., in [5]) to understand the structure of the TDCS failed in the initial stages, indicating that the relativistic $(e,2e)$ process is much more subtle than one might have anticipated from the results for integrated cross sections.

The key to understanding the inner shell ionization process lies in the fact, only appreciated in recent years, that elastic scattering of the active electrons in the effective electrostatic potential, generated by the target nucleus and the spectator electrons, plays an extremely important role [6]. Specifically, only the development of a theoretical description (the relativistic distorted wave Born approximation (RDWBA) [7,8]) including (i) ionizing transitions by virtue of exchange of a longitudinal or transverse photon between the active electrons, and (ii) the representation of the free electrons involved in the process by exact elastic scattering eigenfunctions of the Dirac equation with an effective potential generated by the residual ion, has led to an adequate representation of the experiments.

In a recent theoretical study [9] (referred to as I) a detailed interpretation of one specific $(e,2e)$ experiment [10] on the K shell of copper in terms of interference between longitudinal and transverse ionization amplitudes, and elastic scattering from the residual ion was proposed. The present investigation was stimulated by new experimental data [11] that extend the results of [10] systematically into the high-Z regime. The dependence of the TDCS on atomic number, that is revealed by these experiments, is the topic of the present theoretical study. The dependence of the spin asymmetry on atomic number is also discussed. It can be studied in $(e,2e)$ experiments with transversely polarized relativistic electrons.

II. THEORETICAL BACKGROUND

In the following, we establish some properties of the relativistic $(e,2e)$ processes to be discussed, and also briefly summarize the formalism underlying our RDWBA calculations.

A. Characterization of $(e,2e)$ processes in Ehrhardt geometry

In the present study, we will exclusively consider $(e,2e)$ processes involving the $1s_{1/2}$ electrons of many-electron atoms in coplanar asymmetric unequal energy sharing (''Ehrhardt'') geometry [12]. This arrangement is depicted in Fig. 1, which also introduces our notation. The target state (ionization potential V_b) is ionized by a high energy electron (impact kinetic energy $T_0 \gg V_b$), and a fast electron (momentum $\mathbf{k}_1$) is detected under a fixed angle $\theta_1 < 0$ [13]. The triply differential cross section

$$\frac{d^3\sigma_{(e,2e)}}{d\Omega_1\, d\Omega_2\, dE} \tag{1}$$

is displayed as function of the observation angle θ_2 of the slow electron ($k_2 \ll k_1$). The quantities k_i and T_i ($i = 0,1,2$) are related by the usual relativistic free particle dispersion relation

*Author to whom correspondence should be addressed. Electronic address: keller@th.physik.uni-frankfurt.de

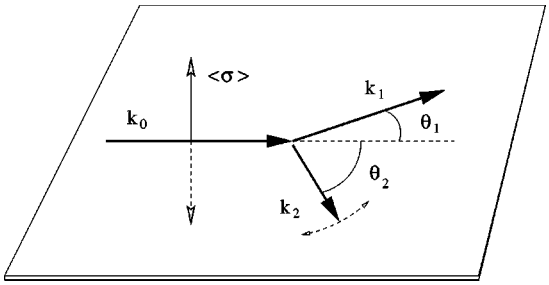

FIG. 1. Schematic representation of an $(e,2e)$ experiment in a coplanar asymmetric unequal energy sharing geometry. The triply differential cross section is measured as function of θ_2. The arrows perpendicular to the scattering plane labeled with $\langle\sigma\rangle$ represent the orientations of incident electron spin expectation value in experiments with tranversely polarized beams.

$$T_i + c^2 = \sqrt{k_i^2 c^2 + c^4} \tag{2}$$

(in atomic units, $\hbar = m_e = e = 1$, $c = 137.035\,989\,5$). As indicated in Fig. 1, such experiments may also be carried out with transversely polarized electrons. The corresponding additional observable is the ''spin asymmetry''

$$A := \frac{d^3\sigma(\uparrow) - d^3\sigma(\downarrow)}{d^3\sigma(\uparrow) + d^3\sigma(\downarrow)}, \tag{3}$$

i.e., the normalized difference of the TDCS obtained with ''spin-up'' and ''spin-down'' electrons.

The main characteristic of the Ehrhardt geometry is the fact that the direct process, which results in the ejected electron being observed at the lower energy T_2, is much more likely than the exchange process involving a large energy transfer to this electron. Therefore the fast electron may for all practical purposes be identified with the projectile. Consequently, the ratio between the magnitude of the momentum transfer $\mathbf{\Delta} := \mathbf{k}_0 - \mathbf{k}_1$ to the target and the relevant intrinsic momentum of the target (pictorially speaking, the Bohr velocity in the initial bound state) is a characteristic parameter of these processes [12].

If one wishes to compare Z-dependent signatures of the ionization process, a definition of ''equivalent scattering kinematics'' is required to account for the differences in the ionization potential. The simplest case of the hydrogen isoelectronic sequence suggests the use of Coulomb units defined by

$$[r] \sim Z^{-1}, \quad [k] \sim Z, \quad [E] \sim Z^2 \tag{4}$$

in order to relate data for different targets. This scaling procedure is, however, only approximately valid for neutral targets because screening by the passive electrons introduces another length scale, reflected in deviations of the experimental inner shell binding energies from the Coulomb scaling behavior. To circumvent this problem, Ehrhardt and coworkers [12] suggested comparing experiments with a fixed ratio T_0/V_b. By contrast, the recent experiments [10,11] used a fixed impact kinetic energy T_0 of 300 keV for all target systems, and compensated the differences in binding energy by varying the detection energy of the fast (scattered) electron, so that the kinematics of the individual measurements are *not* equivalent. While this procedure was enforced by experimental constraints, we argue below that it is also more adequate than the two scaling prescriptions discussed.

In all relativistic problems, the velocity of light, c, appears as an invariable scale parameter. Technically speaking, there is no scale invariant and Lorentz covariant theory of massive particles (see, e.g., [14], Chap. 13). Specifically, the importance of relativistic effects in $(e,2e)$ processes is characterized by the ratios V_b/c^2 and T_i/c^2, so that rescaling the kinetic energies T_i with Z^2 or V_b amounts to also varying the importance of relativistic effects. In fact, it is impossible to disentangle relativistic and atomic-number-dependent effects using *any* scaling procedure. For the study of Z dependences in relativistic $(e,2e)$ collisions, it is therefore advisable to use similar asymptotic energies for all target systems in order to render the results comparable at least with regard to the importance of relativistic effects. As V_b/c^2 is a target property, the natural choice would be to vary the impact energy accordingly (i.e., work at fixed excess energy) in order to minimize the changes in T_i/c^2. However, in Ehrhardt geometry $(T_0 \gg V_b, T_1 \gg T_2)$ this procedure may reasonably be simulated by varying the detection energy of the fast (scattered) electron, as in the recent experiments [10,11]. We will restrict the present discussion to this case.

In the relativistic context, the classification of $(e,2e)$ processes in terms of the magnitude of scaled momentum transfer is thus bound to play a subordinate role. In view of its importance in nonrelativistic $(e,2e)$ theory, it is nevertheless worth mentioning that in all relativistic $(e,2e)$ processes under consideration, the scaled momentum transfer is of order unity. This implies that the the interpretation of Ehrhardt and co-workers [12] (ultimately based on the seminal work of Bethe [15]), that relates $(e,2e)$ reactions at very small momentum transfer $\mathbf{\Delta}$ to ionization by dipole photon absorption, and collisions with very large momentum transfer to impulsive Compton-like processes, is not very helpful here.

B. Outline of theoretical formalism

The TDCS for ionization of one of the $(2j_b+1)$ electrons of a closed shell with total angular momentum j_b (or quantum number κ_b) is given by

$$\frac{d^3\sigma_{(e,2e)}}{d\Omega_1\, d\Omega_2\, dE} = (2\pi)^4 \frac{k_1 k_2}{k_0} \frac{E_0 E_1 E_2}{c^6} \frac{1}{2} \times \sum_{\epsilon_1 \epsilon_0 \epsilon_2 \epsilon_b} |T(k_1\epsilon_1, k_2\epsilon_2; k_0\epsilon_0, \kappa_b\epsilon_b)|^2, \tag{5}$$

where the quantities ϵ denote the spin and angular momentum projections of continuum and bound electron states, respectively, and $T(k_1\epsilon_1, k_2\epsilon_2; k_0\epsilon_0, \kappa_b\epsilon_b)$ is the scattering T matrix.

As it is not possible to define a manifestly covariant many-body Hamilton operator for a relativistic Coulomb system, a consistent theory of the T matrix for relativistic $(e,2e)$ processes can only be formulated via the perturbation expansion of quantum electrodynamics (see, e.g., [14]). As noted above, it is adequate to represent the action of the passive electrons and the atomic nucleus on the active electrons by a

classical effective potential. The leading (first-) order contribution to the perturbation expansion of the $(e,2e)T$ matrix in the Furry picture (see, e.g., [14]) defined by this potential, describes ionization by exchange of one virtual photon between the incident and the initially bound electron. This quantity is the RDWBA T matrix (written in the conventions of [14]):

$$\begin{aligned} T(k_1,\epsilon_1;k_2,\epsilon_2;k_0,\epsilon_0;\kappa,\epsilon_b) &= T^{dir}-T^{ex} \\ &= \int d^3x\ \overline{\psi}^{(-)}_{\mathbf{k}_1,\epsilon_1}(\mathbf{x})\gamma^\mu\psi^{(+)}_{\mathbf{k}_0,\epsilon_0}(\mathbf{x}) \\ &\quad\times\int d^3y\ D^0_{\mu\nu}(\mathbf{x}-\mathbf{y})\overline{\psi}^{(-)}_{\mathbf{k}_2,\epsilon_2}(\mathbf{y})\gamma^\nu\psi_{\kappa,\epsilon_b}(\mathbf{y}) \\ &\quad-\int d^3x\ \overline{\psi}^{(-)}_{\mathbf{k}_2,\epsilon_2}(\mathbf{x})\gamma^\mu\psi^{(+)}_{\mathbf{k}_0,\epsilon_0}(\mathbf{x}) \\ &\quad\times\int d^3y\ D^0_{\mu\nu}(\mathbf{x}-\mathbf{y})\overline{\psi}^{(-)}_{\mathbf{k}_1,\epsilon_1}(\mathbf{y})\gamma^\nu\psi_{\kappa,\epsilon_b}(\mathbf{y}). \end{aligned} \tag{6}$$

It is equivalent to the Møller T matrix element [1], with an exact bound eigenstate ψ_{κ,ϵ_b} and exact continuum eigenstates $\psi^{(\pm)}_{\mathbf{k},\epsilon}$ (satisfying appropriate scattering boundary conditions) of the Dirac equation with the effective potential of the residual ion. Further technical details can be found in [8]. A simplified model, the relativistic first-order Born approximation (RFBA) is obtained by neglecting the elastic scattering of the projectile electron in the effective potential of the spectator ion, i.e., by replacing the continuum states $\psi^{(\pm)}_{\mathbf{k},\epsilon}$ depending on $\mathbf{x}$ in Eq. (6) with Dirac plane wave states [16].

Equation (6) represents the interaction between the transition four currents j^μ_{10} of the projectile electron and j^ν_{2b} of the ejected electron mediated by the free photon Green's function $D^0_{\mu\nu}(\mathbf{x}-\mathbf{y})$, so that, e.g.,

$$T^{dir}\sim\int d^3x\ j^\mu_{10}(\mathbf{x})\int d^3y\ D^0_{\mu\nu}(\mathbf{x}-\mathbf{y})j^\nu_{2b}(\mathbf{y}). \tag{7}$$

Resolving the four currents into (timelike) density components $j^0=\rho$ and spatial currents $\mathbf{j}=(j^1,j^2,j^3)$ and using a gauge (e.g., Feynman or Coulomb gauge) in which $D_{0i}=D_{i0}=0$, the contributions to the first-order T matrix may be rewritten as, e.g.,

$$\begin{aligned} T^{dir}\sim&\int d^3x\ \rho_{10}(\mathbf{x})\int d^3y\ D^0_{00}(\mathbf{x}-\mathbf{y})\rho_{2b}(\mathbf{y}) \\ &-\int d^3x\ j^i_{10}(\mathbf{x})\int d^3y\ D^0_{ik}(\mathbf{x}-\mathbf{y})j^k_{2b}(\mathbf{y}) \\ =&\,T^{long}-T^{trans}. \end{aligned} \tag{8}$$

T^{long} describes interactions by exchange of a longitudinal photon. T^{trans} represents transverse photon exchange, in particular the relativistic electromagnetic coupling of the spatial charge currents of the two active electrons [17].

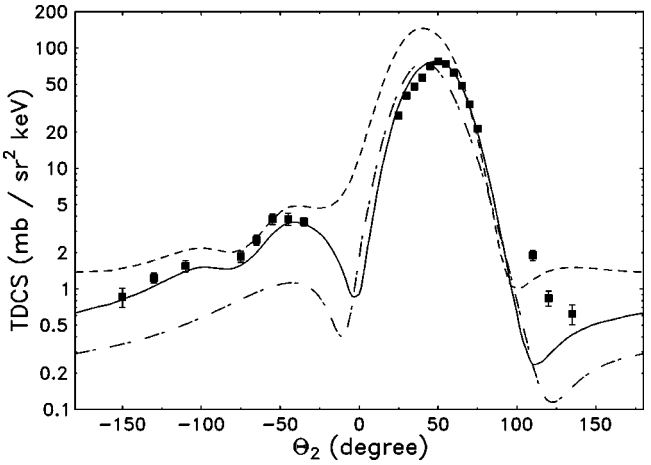

FIG. 2. TDCS for $(e,2e)$ on the K shell of copper ($Z=29$). Impact energy $T_0=300$ keV, slow outgoing electron energy $T_2=71$ keV, fast electron observation angle $\theta_1=-9°$. Symbols: relative experimental data [10], normalized to RDWBA calculation at the maximum; full curve: result of RDWBA calculation [18]; dashed curve: result of RDWBA calculation including only longitudinal term [9]; dash-dotted curve: result of RFBA calculation [9].

III. ATOMIC NUMBER DEPENDENCE OF TDCS

A. Ionization of the K shell of copper

The initial experiment of Besch *et al.* [10] was carried out on the K electrons of copper. In Fig. 2, we show these experimental results in comparison with results of the RDWBA and the RFBA. The relative experimental data indicate a double peak structure for emission of both electrons into the same half-plane (negative values of θ_1 and θ_2). Except for the three data points at large positive θ_2, the measured TDCS is well reproduced by the RDWBA calculation of [18]. Since in this experiment the ionization potential ($V^{Z=29}_{1s_{1/2}}=8.979$ keV) was much smaller than the impact kinetic energy, the effects of the projectile-spectator ion interaction can be estimated using perturbation theory. A corresponding detailed study was presented in I. The main results of this work can be summarized as follows: (i) The secondary maximum of the TDCS for emissions of both electrons into the same quadrant is due to the destructive interference of the amplitudes T^{long} and T^{trans}. This effect is also present qualitatively in the RFBA result. (ii) The additional structure at $\theta_2\sim-95°$ is caused by elastic scattering of the projectile electron in the spectator ion potential, followed by an ionizing electron-electron collision without momentum transfer to the spectator ion. This structure also appears in a RDWBA-type calculation that neglects T^{trans} [19].

The model calculation just mentioned also shows some extra structure in the region of the ''interference peak,'' indicating that in this angular regime, the magnetic interaction between the projectile electron and the spectator ion cannot be ignored [9]. Moreover, as was shown in [20], the position of the binary maximum cannot be reproduced using a plane-wave description of the projectile electron (RFBA).

B. Ionization of the K shell of silver

Sauter *et al.* [11] have very recently extended the measurements of [10] to silver and gold targets. Figure 3 (upper

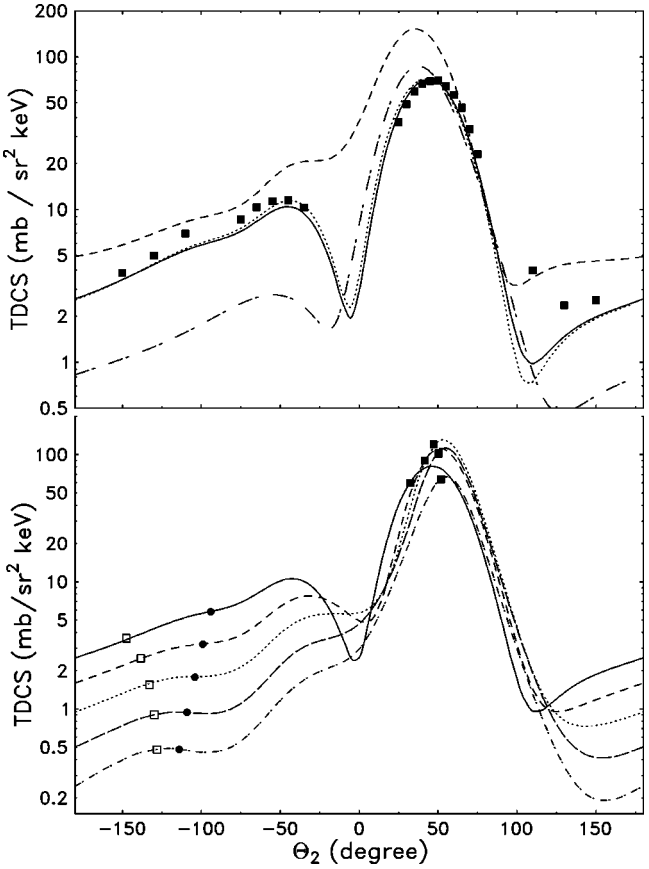

FIG. 3. TDCS for (*e*,2*e*) on the *K* shell of silver ($Z=47$). Impact energy $T_0=300$ keV. Top, slow outgoing electron energy $T_2=71$ keV, fast electron observation angle $\theta_1=-9°$. Symbols, relative experimental data [11] normalized to RDWBA calculation at the maximum; full curve, result of RDWBA calculation; dashed curve: result of RDWBA calculation including only longitudinal term; dotted curve, result of RDWBA calculation including only direct term; dash-dotted curve, result of RFBA calculation. Bottom, RDWBA results for slow outgoing electron energy of 70 keV and different observation angles. Full curve, $\theta_1=-10°$; short dashed curve: $\theta_1=-15°$; dotted curve, $\theta_1=-20°$; long dashed curve, $\theta_1=-25°$; dash-dotted curve, $\theta_1=-30°$. full squares, direction of momentum transfer; open squares, $(-)$ direction of momentum transfer; full circles, ''critical angle'' for double scattering (see text).

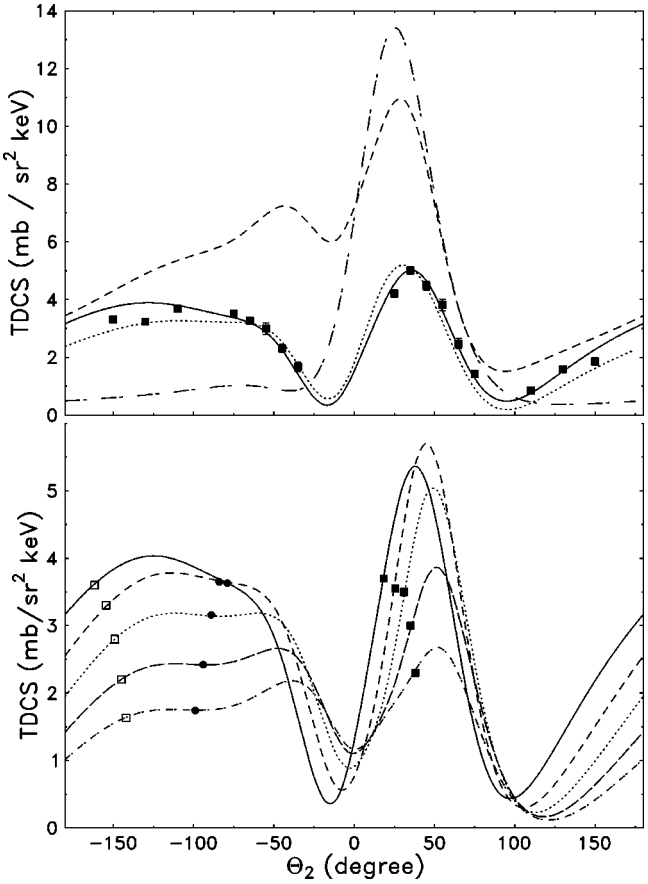

FIG. 4. Same as Fig. 3, but for a gold ($Z=79$) target.

part) shows their results for silver along with data from the same theoretical models as in Fig. 2. The two sets of results are remarkably similar, indicating that the basic physical mechanisms discussed in I can also be invoked to explain inner shell (*e*,2*e*) reactions on silver. This result is not unexpected in view of the relatively small ionization potential involved ($V_{1s_{1/2}}^{Z=47}=25.514$ keV). The lower part of Fig. 3 shows that the secondary maximum for large negative θ_2 becomes more pronounced as θ_1 takes larger absolute values (an effect that would be interesting to study experimentally) [21]. The shift of its position follows the prediction of the simple double scattering model used in I (full circles). This result emphasizes the fact that the structure in question is unrelated to the conventional ''recoil peak'' due to backscattering of the ionized electron [22], that would appear opposite to the direction of momentum transfer.

On the other hand, the upper part of Fig. 3 also shows that a nonperturbative inclusion of the projectile-spectator ion interaction becomes more and more important as *Z* is increased at a given impact energy. Indeed, the RFBA model fails to reproduce the absolute magnitude of the RDWBA cross section, in contrast to the case of copper. Moreover, the calculated double scattering signature is less pronounced, indicating that higher-order processes become more important. Like for copper, the massive shift of the binary maximum with respect to the direction of momentum transfer is only reproduced by the full RDWBA calculation. Finally, the contribution of the exchange amplitude T^{ex} plays a subordinate role, as was mentioned above [23].

C. Ionization of the *K* shell of gold

The results of [11] for a gold target (Fig. 4) differ dramatically from those discussed so far (note the linear rather than logarithmic scale). The secondary maximum is similar in absolute magnitude to the binary one, and has the shape of a broad plateau; this effect has been predicted within the RDWBA model [8]. The agreement of the RDWBA calculation with the experimental results is very good in the forward half-plane (and, remarkably, also for very large positive θ_2, in contrast to the data sets for copper and silver), but the experiment shows a shallow minimum of the TDCS in the backward emission region where the calculation predicts the maximum of the secondary peak.

A comparison of the different calculations shows some additional peculiarities. The result of the RFBA calculation

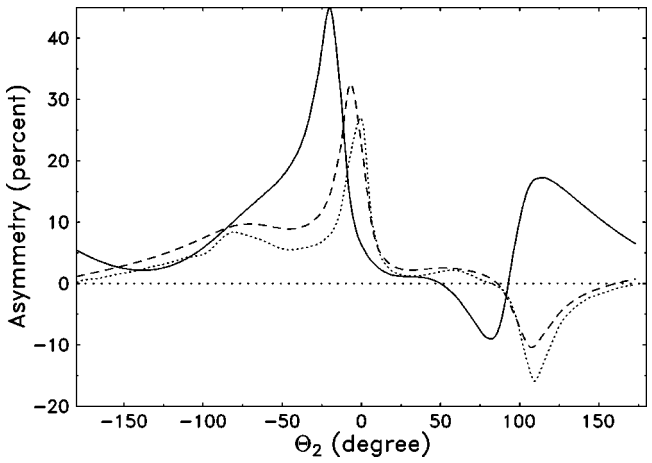

FIG. 5. Spin asymmetries for electron impact ionization of the $1s_{1/2}$ state, as function of slow electron observation angle, calculated in RDWBA. Impact energy $T_0=300$ keV, slow electron observation energy $T_2=71$ keV, fast electron observation angle $\theta_1=-9°$. Full curve, gold target; dashed curve, silver target; dotted curve, copper target.

has no similarity with the measured data, indicating an overwhelming influence of the projectile-spectator ion interaction. Also, exchange effects play a more important role than for the lighter target systems. In particular, they significantly influence the shape of the calculated TDCS for $\theta_2<-90°$. These observations are readily explained in terms of the large ionization potential of the K electrons of gold ($V_{1s_{1/2}}^{Z=79}=80.7$ keV): the ratio of impact energy and ionization potential is too small to warrant the applicability of a perturbative treatment of projectile scattering, and the ratio of the outgoing electron kinetic energies ($T_1/T_2\approx 2.1$) is too small for a typical ''Ehrhardt''-type situation. It is also interesting to observe that T^{long} alone dictates the shape of the TDCS for $|\theta_2|>120°$ (backward emission), whereas the inclusion of T^{trans} is essential for reproducing the plateau structure.

The changes in the shape of the TDCS as function of θ_1 (lower part of Fig. 4) shed some light on these observations. For larger absolute values of θ_1, the double-peak structure of the TDCS for negative θ_2 observed in Fig. 3 reemerges, and the peak close to the forward direction is shifted towards $\theta_2=0°$ (where it eventually merges with the binary peak, as demonstrated in [24], Fig. 5). The ''interference peak'' in Fig. 3 follows the same pattern. In the RFBA calculation, one obtains a small hump in this region (upper part of Fig. 4) that shows the same trend when analyzed as function of θ_1 (data not shown). We therefore conclude that the left part of the broad secondary structure is again in large part due to the interference mechanism discussed in I.

On the other hand, the double scattering analysis of the large-θ_2 behavior of the TDCS is obviously inapplicable: this picture would predict a maximum where a minimum between the two secondary peaks develops at larger absolute values of θ_1 (full circles). It does not allow to predict the changes in position of these structures. This demonstrates that a perturbative approach to describing projectile scattering effects in the inner shell ionization of high-Z targets like gold is not possible in this regime of impact energies, whereas the all-order treatment of elastic scattering effects in RDWBA accounts for all major features of the measured TDCS.

IV. ATOMIC NUMBER DEPENDENCE OF SPIN ASYMMETRY

For $(e,2e)$ experiments on s states at nonrelativistic energies, the spin asymmetry defined by Eq. (3) is strictly zero unless the target is prepared in a polarized state [24]. The nonzero asymmetry measured by Prinz, Besch, and Nakel [25] in $(e,2e)$ scattering on the K shell of silver must therefore be attributed to relativistic effects. Indeed, these authors interpreted their results in terms of relativistic spin-orbit coupling of the continuum electrons, i.e., Mott scattering of the unbound electrons in the strong external field generated by the spectator ion. The experimental observation that the asymmetry is small in the region of the binary peak, and larger in the region of the secondary maximum, is in agreement with the standard semiclassical picture in which the binary (''recoil'') peak is due to electron-electron scattering without (with) momentum transfer to the spectator ion [25]. This interpretation was confirmed by the good agreement of the experimental data with RDWBA calculations, that include elastic scattering in the effective potential generated by the spectator ion to all orders [24]. Moreover, first-order calculations ignoring elastic scattering in all continuum states [26] predict vanishing spin asymmetries also in the relativistic domain. Hence relativistic effects in the elastic scattering of the electrons in the spectator ion field are ultimately responsible for the spin asymmetries observed.

It was argued in [24] that asymmetries induced by continuum spin-orbit coupling should be strongly Z dependent. Comparison of calculated asymmetries for different target systems on the basis of the V_b scaling described in Sec. II A, showed the expected increase of the asymmetry with Z for all angles. The experimental verification of this effect was proposed as a strong test of the continuum spin-orbit coupling interpretation. However, as was shown in Sec. II A, this line of reasoning is inconclusive because in V_b scaling, the importance of all relativistic effects is increased along with Z. Therefore, it is advisable to reconsider the Z dependence of the asymmetry for fixed impact energy.

Figure 5 shows asymmetries calculated in RDWBA for the three atomic targets discussed in the previous section. Corresponding experiments are currently being carried out [27]. We predict that the asymmetry function increases with atomic number in the angular regime $-100°<\theta_2<-30°$ considered in [24,25], and is close to zero in the binary regime. This is consistent with the semiclassical argument of [25]. Our present calculations suggest, however, that the asymmetry for the heaviest target, gold, is *smaller* than the result for silver in the region of the backward maximum ($-150°<\theta_2<-85°$) of the gold TDCS (compare Figs. 3 and 4). This effect did not manifest itself in the V_b scaled data of [24], indicating that it is of relativistic rather than strong-field origin. As we could attribute the large TDCS in this regime to the strong elastic rescattering in the ionic field of the high-Z atom (see Sec. III), we conclude that the interpretation in terms of continuum spin-orbit coupling alone does not suffice to explain these spin asymmetries.

Some insight into this phenomenon may be obtained by

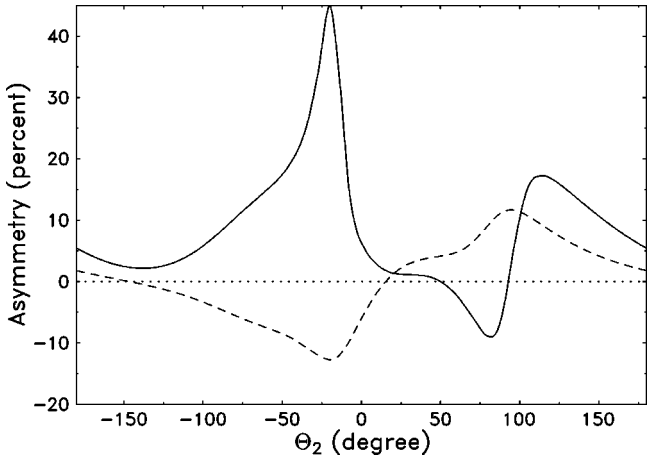

FIG. 6. Spin asymmetries for electron impact ionization of the $1s_{1/2}$ state of gold, kinematics as in Fig. 5. Full curve, of RDWBA calculation; dashed curve, RDWBA calculation with longitudinal amplitude only.

considering the RDWBA asymmetry obtained from the longitudinal scattering amplitude only. Remarkably, Fig. 6 shows that the strongest deviations from the full RDWBA result occur for observation of both electrons in the same quadrant. Comparison with Fig. 4 (upper part) shows that in this region the effect of the transverse ionization amplitude is

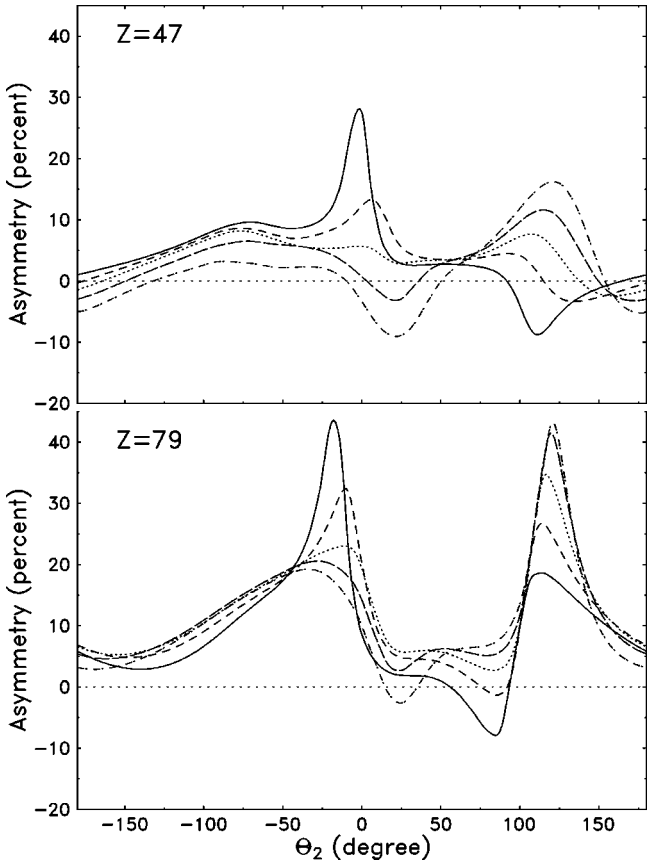

FIG. 7. Spin asymmetries for electron impact ionization of the $1s_{1/2}$ state, as function of slow electron observation angle, calculated in RDWBA. Impact energy $T_0=300$ keV, slow electron observation energy $T_2=70$ keV, different θ_1 (identification of curves as in Fig. 3). Top, silver target; bottom, gold target.

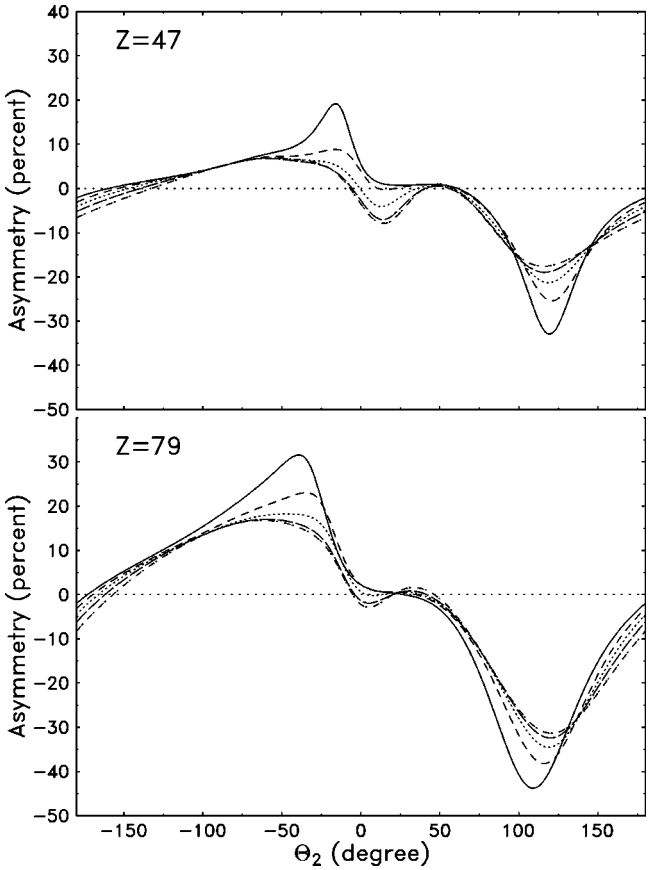

FIG. 8. Same as Fig. 7, but results of RFBA calculations.

indeed most pronounced. Hence we find that the expected increase of the spin asymmetry with Z manifests itself only in the angular region where the current-current interaction of the electrons plays an important role.

However, as discussed above (see also [9]), the magnetic projectile-spectator ion coupling is effective in the same angular regime ($-90°<\theta_1,\theta_2<0°$). In order to disentangle these effects, we compare, for five different fast electron observation angles, asymmetries for ionization of the K electrons of silver and gold calculated with RDWBA (Fig. 7) and RFBA (Fig. 8). The asymmetries predicted by the first-order Born calculation are essentially independent of the fast electron observation angle over the whole angular range (except in the region of the strong TDCS minima, where the sharp maxima in the asymmetry are an artifact of the definition of the asymmetry, see [24]). This is consistent with the continuum spin-orbit coupling interpretation of the asymmetry: the kinematics of ejected electron rescattering in the ionic potential are the same for all fast electron observation angles, while any influence of the kinematics of the electron-electron scattering process should result in a dependence of the asymmetry on momentum transfer. The RDWBA data strongly fluctuate as a function of θ_1 except for $-150°<\theta_2<-50°$. This indicates that here the nonvanishing asymmetry is in large part due to Mott scattering of the ejected electron in the field of the atomic nucleus, whereas spin effects due to the projectile-spectator ion interaction play no important role. All calculations show very small asymmetries in the region of the binary peak, again confirming the essence of the interpretation put forward in [25].

V. CONCLUSIONS

The different features of $(e,2e)$ TDCS for different target systems observed in recent experiments in coplanar asymmetric geometry [11] can be explained in terms of the mechanisms included in the RDWBA model, namely, Mott scattering of the active electrons in the field of the spectator ion, and interference of the amplitudes for longitudinal and transverse single-photon exchange. Even at very high atomic numbers, the interference mechanism plays a key role for emission of both electrons into the same quadrant. For $T_0, T_1, T_2 \gg V_b$, a perturbative treatment of projectile rescattering suffices for a qualitative interpretation. Strong nonperturbative features show up for lower relative kinetic energies, or high Z.

The spin asymmetry of relativistic $(e,2e)$ processes on s states is essentially due to continuum spin-orbit coupling (Mott scattering of the individual free electrons), but the measured asymmetries are also influenced by the interplay of longitudinal and transverse interaction between the two active electrons. Our present calculations provide evidence that a large contribution of the transverse amplitude is a precondition for observing large asymmetry values, in particular the expected Z dependence. The details of the relation between the spin effects in electron-electron scattering and electron-spectator ion scattering in the different asymptotic channels, which conspire to determine the spin asymmetries measured in $(e,2e)$ experiments, remain to be understood.

Note added in proof. After submission of the present paper, Sauter *et al.* completed and published their measurements of the spin asymmetries discussed in Sec. IV [27]. The experimental results are in quantitative agreement with the predictions of Fig. 5.

ACKNOWLEDGMENTS

We would like to thank M. Sauter and W. Nakel for many exciting and fruitful discussions.

[1] C. Møller, Z. Phys. **70**, 786 (1931).
[2] H. Bethe, Z. Phys. **76**, 293 (1933).
[3] B. L. Moiseiwitsch, Adv. At. Mol. Phys. **16**, 281 (1980).
[4] E. Schüle and W. Nakel, J. Phys. B **15**, L539 (1982).
[5] R. M. Dreizler, H. R. J. Walters, C. T. Whelan, H. Ast, and S. Keller, in *Coincidence Studies of Electron and Photon Impact Ionization*, edited by C. T. Whelan and H. R. J. Walters (Plenum, New York, 1997), p. 199.
[6] X. Zhang, C. T. Whelan, H. R. J. Walters, R. J. Allan, P. Bickert, W. Hink, and S. Schönberger, J. Phys. B **25**, 4325 (1992).
[7] H. Ast, S. Keller, C. T. Whelan, H. R. J. Walters, and R. M. Dreizler, Phys. Rev. A **50**, R1 (1994).
[8] S. Keller, C. T. Whelan, H. Ast, H. R. J. Walters, and R. M. Dreizler, Phys. Rev. A **50**, 3865 (1994).
[9] S. Keller and R. M. Dreizler, Phys. Rev. A **57**, 3652 (1998).
[10] K. H. Besch, M. Sauter, and W. Nakel, J. Phys. B **30**, L73 (1997).
[11] M. Sauter, N. Keller, and W. Nakel, J. Phys. B **31**, 2947 (1998).
[12] H. Ehrhardt, Comments At. Mol. Phys. **13**, 115 (1983); H. Ehrhardt, K. Jung, G. Knöth, and P. Schlemmer, Z. Phys. D **1**, 3 (1986).
[13] Notice that we use a definition of the coplanar angles θ_i in $(-\pi,\pi]$ that is related to conventional spherical coordinates (r_s,θ_s,ϕ_s) by $\theta=\theta_s \cos\phi_s$.
[14] C. Itzykson and J. B. Zuber, *Quantum Field Theory* (McGraw-Hill, New York, 1980).
[15] H. Bethe, Ann. Phys. (Leipzig) **5**, 325 (1930).
[16] S. Keller, R. M. Dreizler, L. U. Ancarani, H. R. J. Walters, H. Ast, and C. T. Whelan, Z. Phys. D **37**, 191 (1996).
[17] For example, in Coulomb gauge, D_{00} is the usual Coulomb interaction, whereas D_{ij}, the ''generalized Breit interaction,'' includes all magnetic and retardation effects.
[18] R. M. Dreizler, H. Ast, S. Keller, C. T. Whelan, L. U. Ancarani, and H. R. J. Walters, J. Phys. B **30**, L77 (1997).
[19] The same effect has previously been observed in coplanar symmetric and perpendicular plane geometries at nonrelativistic energies. See X. Zhang, C. T. Whelan, and H. R. J. Walters, J. Phys. B **23**, L173 (1990); **23**, L509 (1990), and references therein.
[20] H. Ast, S. Keller, R. M. Dreizler, C. T. Whelan, L. U. Ancarani, and H. R. J. Walters, J. Phys. B **29**, L585 (1996).
[21] The results shown in the lower part of Figs. 3 and 4, as well as in Figs. 7 and 8, have been obtained before the kinematics of the experiment [11] were determined, hence the slightly different energy sharings. It is obvious, and has been explicitly verified, that the differences in calculated TDCS and asymmetries are negligible.
[22] See, e.g., H. R. J. Walters, Phys. Rep. **116**, 1 (1984); J. S. Briggs, Comments At. Mol. Phys. **23**, 155 (1989).
[23] For the copper case, the exchange contribution is still smaller, see [9].
[24] S. Keller, R. M. Dreizler, H. Ast, C. T. Whelan, and H. R. J. Walters, Phys. Rev. A **53**, 2295 (1996).
[25] H.-Th. Prinz, K.-H. Besch, and W. Nakel, Phys. Rev. Lett. **74**, 243 (1995).
[26] S. Keller and C. T. Whelan, J. Phys. B **27**, L771 (1994).
[27] M. Sauter, H. Ott, and W. Nakel, J. Phys. B **31**, 2967 (1998).